



Title	Physico-chemical Behavior of Hydrogen Sulfide Induced by Reactions with H and D Atoms on Different Types of Ice Surfaces at Low Temperature
Author(s)	Oba, Yasuhiro; Tomaru, Takuto; Kouchi, Akira; Watanabe, Naoki
Citation	Astrophysical journal, 874(2), 124 <a href="https://doi.org/10.3847/1538-4357/ab0961">https://doi.org/10.3847/1538-4357/ab0961</a>
Issue Date	2019-04-01
Doc URL	<a href="http://hdl.handle.net/2115/77214">http://hdl.handle.net/2115/77214</a>
Rights	This is an author-created, un-copyrighted version of an article accepted for publication/published in Astrophysical journal. IOP Publishing Ltd is not responsible for any errors or omissions in this version of the manuscript or any version derived from it. The Version of Record is available online at <a href="https://doi.org/10.3847/1538-4357/ab0961">10.3847/1538-4357/ab0961</a> .
Type	article (author version)
File Information	Astrophysical journal874(2)_124-.pdf



[Instructions for use](#)

1 Physico-chemical behavior of hydrogen sulfide induced by reactions with H and D  
2 atoms on different types of ice surfaces at low temperatures

3

4 Short title: Reactions of H<sub>2</sub>S with H and D atoms on ices

5

6 Yasuhiro Oba\*, Takuto Tomaru, Akira Kouchi, and Naoki Watanabe

7 Institute of Low Temperature Science, Hokkaido University, N19W8, Kita-ku, Sapporo,

8 Hokkaido 060-0189 JAPAN

9

10 \* Corresponding author: oba@lowtem.hokudai.ac.jp

11

12 Abstract

13 To elucidate the physico-chemical behavior of hydrogen sulfide (H<sub>2</sub>S) on icy grains in  
14 dense molecular clouds, we investigated the surface reactions of solid H<sub>2</sub>S with H and D  
15 atoms in low-temperature laboratory experiments. We confirmed that H<sub>2</sub>S was lost from  
16 the surface by reaction with H atoms via chemical desorption. We found no strong  
17 association between the effective desorption cross section and the ice structure (porous  
18 amorphous, non-porous amorphous, or crystalline) or temperature (10–30 K). At 10 K,

1 the reaction rate constant for the H–D substitution of solid H<sub>2</sub>S with D atoms almost  
2 matched that for the D–H substitution of solid D<sub>2</sub>S with H atoms. The present  
3 experimental results clearly suggest that the observed abundances of H<sub>2</sub>S and its  
4 deuterated isotopologues (HDS and D<sub>2</sub>S) in the interstellar medium are controlled, at  
5 least partly, by surface reactions on interstellar icy grains.

6

7 Key words: astrochemistry — ISM: molecules — ISM: clouds

8

## 9 1. Introduction

10 Hydrogen sulfide (H<sub>2</sub>S) is one of the most primitive sulfur-bearing molecules  
11 detected in the interstellar medium (ISM). Since its first detection in W3 and NGC 7538,  
12 and five other Galactic regions (Thaddeus et al. 1972), H<sub>2</sub>S has been detected in the gas  
13 phases of various interstellar sources, such as cold dark clouds (Minh et al. 1989),  
14 diffuse clouds (Neufeld et al. 2015), hot cores (Hatchell et al. 1998), star-forming  
15 regions (Wakelam et al. 2004), low-mass protostars (van Dishoeck et al. 1995; Vastel et  
16 al. 2003), and a protoplanetary disk (Phuong et al. 2018). By contrast, the presence of  
17 solid-state H<sub>2</sub>S remains debatable. Geballe et al. (1985) reported solid H<sub>2</sub>S in the  
18 infrared spectrum of a high-mass protostar W33A. However, because of the faint

1 infrared feature of the possible H<sub>2</sub>S band at 3.9 μm, the presence of solid-state  
2 interstellar H<sub>2</sub>S in this source is inconclusive and is not universally accepted in the  
3 astrochemical community (e.g., Garrod et al. 2007; Jiménez-Escobar & Muñoz Caro  
4 2011).

5 As the observed interstellar abundance of H<sub>2</sub>S cannot be explained by  
6 gas-phase synthesis alone, it is thought to be mainly formed by successive additions of  
7 H atoms to S atoms on icy grains (Millar et al. 1986; Millar & Herbst 1990):



10 As reactions (1) and (2) are barrierless, H<sub>2</sub>S is easily formed on icy grains even at  
11 extremely low temperatures (~10 K). When H<sub>2</sub>S remains on the grains, it can further  
12 react with H atoms as follows:



14 which has a moderate activation barrier of approximately 1500 K (Lamberts & Kästner  
15 2017). The HS radicals revert to H<sub>2</sub>S via reaction (2). Garrod et al. (2007) attributed the  
16 abundant gas-phase H<sub>2</sub>S to desorption of the H<sub>2</sub>S formed by reaction (2). This  
17 mechanism, here called *chemical desorption*, is also known as reactive desorption.  
18 Chemical desorption is a non-thermal desorption mechanism that operates through the

1 heat of exothermic reactions on grains. Chemical desorption was pioneered by the  
2 modeling community to explain the gas-phase abundances of molecules derived from  
3 icy grains at low temperatures (Garrod et al. 2007; Cuppen et al. 2017). Recently, it has  
4 been experimentally demonstrated on several molecules (Dulieu et al. 2013; He et al.  
5 2017; Chuang et al. 2018; Oba et al. 2018). Using Fourier-transform infrared (FTIR)  
6 spectroscopy, we recently quantified the chemical desorption of H<sub>2</sub>S and H atoms  
7 reacting on the surface of amorphous solid water (ASW) at 10 K (Oba et al. 2018). In  
8 that experiment, the H<sub>2</sub>S abundance was reduced through the repetition of reactions (2)  
9 and (3). Clearly, chemical reactions play a dominant role in desorption of H<sub>2</sub>S and/or  
10 HS into the gas phase.

11 To further elucidate the physico-chemical behavior of H<sub>2</sub>S at low temperatures,  
12 we now react H<sub>2</sub>S with not only H atoms but also D atoms. From the experimental  
13 results, we deduce a possible mechanism for the deuterium enrichment of HS in the  
14 ISM and the dependence of chemical desorption on physical parameters such as the  
15 temperature and structure of the ice.

16

## 17 2. Experiments

### 18 2.1. Apparatus

1           In all experiments, we applied the surface-reaction monitoring system used in  
2 our previous study (Oba et al. 2018). The main components are an ultrahigh vacuum  
3 chamber, a reflection–absorption type FTIR, a quadrupole mass spectrometer (QMS), a  
4 gold-coated substrate connected to a helium cryostat, and an atomic source chamber.  
5 The substrate temperature is controllable between 5 and 280 K inclusive. The base  
6 pressure in the chamber is of the order  $10^{-8}$  Pa.

7

## 8 2.2. Experimental procedure

### 9 2.2.1. H<sub>2</sub>S + H

10           H<sub>2</sub>S was reacted with H atoms on the surfaces of three types of H<sub>2</sub>O ice: porous  
11 (p-) ASW, non-porous (np-) ASW, and polycrystalline water ice (c-H<sub>2</sub>O). The p-ASW  
12 was produced by the vapor-deposition of gaseous H<sub>2</sub>O through a capillary plate inclined  
13 at 45° to the surface normal at 10–30 K. The np-ASW and c-H<sub>2</sub>O were formed similarly,  
14 but at different deposition surface temperatures (90 and 140 K, respectively). The  
15 substrates of the np-ASW and c-H<sub>2</sub>O samples were cooled to 10 K after deposition. The  
16 thickness of each ice was adjusted to approximately 30 monolayers (MLs, where 1 ML  
17 =  $1 \times 10^{15}$  molecules cm<sup>-2</sup>). The deposition rate of the ice was ~2 ML minutes<sup>-1</sup>.  
18 Gaseous H<sub>2</sub>S was deposited through the same capillary plate onto the H<sub>2</sub>O ice at 10–30

1 K for p-ASW and at 10 K for np-ASW and c-H<sub>2</sub>O. The H<sub>2</sub>S thickness (~0.7 ML) was  
2 estimated from the peak area and the band strength of the S–H stretching band at ~2570  
3 cm<sup>-1</sup> ( $8.3 \times 10^{-18}$  cm molecules<sup>-1</sup>; Fathe et al. 2006). The H<sub>2</sub>S deposition rate was ~1  
4 ML minutes<sup>-1</sup>. Hydrogen atoms were produced by dissociating H<sub>2</sub> molecules in a  
5 microwave-induced H<sub>2</sub> plasma in a Pyrex tube. The produced atoms were transferred  
6 through a series of polytetrafluoroethylene and aluminum (Al) tubes, which thermalized  
7 them to ~100 K through multiple collisions with the inner wall of the Al tube (100 K).  
8 Following the method proposed by Oba et al. (2014a), the H-atom flux was estimated as  
9  $5.7 \times 10^{13}$  atoms cm<sup>-2</sup> s<sup>-1</sup>. The reaction was monitored in situ by FTIR for up to 3 hr.  
10 After exposure to H atoms, the abundance of H<sub>2</sub>S remaining on the ice was measured in  
11 temperature-programmed desorption (TPD) experiments using the QMS. As a blank  
12 experiment, the deposited H<sub>2</sub>S (~0.7 ML) was exposed to H<sub>2</sub> molecules for the same  
13 duration. Neither reaction nor desorption was confirmed in the blank, even at 30 K. The  
14 FTIR measurements, TPD experiments, and blank experiments were performed as  
15 described in the following section, unless otherwise noted.

16

### 17 2.2.2. H<sub>2</sub>S + D

18 Approximately 0.7 ML of solid H<sub>2</sub>S was prepared on the surface of p-ASW,

1 np-ASW, or c-H<sub>2</sub>O at 10 K. The preparation method has been described in the previous  
2 section. The ice thickness was adjusted to 30 ML, and the deposited H<sub>2</sub>S was exposed to  
3 D atoms for up to 2 hr at 10 K. The D atoms were produced by dissociating D<sub>2</sub>  
4 molecules in a microwave-induced D<sub>2</sub> plasma, which was cooled to 100 K before  
5 reaction with H<sub>2</sub>S on the ice surface. The estimated flux of D atoms was  $2.5 \times 10^{14}$   
6 atoms cm<sup>-2</sup> s<sup>-1</sup>.

7

### 8 2.2.3. D<sub>2</sub>S + H

9 Gaseous D<sub>2</sub>S was deposited on the surface of porous amorphous deuterated  
10 water (D<sub>2</sub>O, hereafter denoted as p-ASW-d). The p-ASW-d was 30 ML thick at 10 K,  
11 and the solid D<sub>2</sub>S thickness (~0.7 ML) was estimated from the peak area and the  
12 reported band strength of the S–D stretching band of amorphous D<sub>2</sub>S at 1860 cm<sup>-1</sup> ( $4.3$   
13  $\times 10^{-18}$  molecules cm<sup>-1</sup>; Fathe et al. 2006). If the D<sub>2</sub>O is substituted with H<sub>2</sub>O, the D<sub>2</sub>S  
14 deposition can be accompanied by hydrogen–deuterium exchange between H<sub>2</sub>O and  
15 D<sub>2</sub>S in the present experimental set up, causing possible misinterpretations of the results.  
16 Therefore, we applied D<sub>2</sub>O instead of H<sub>2</sub>O in this experiment. The deposited D<sub>2</sub>S was  
17 exposed to a flux of H atoms ( $1.1 \times 10^{14}$  atoms cm<sup>-2</sup> s<sup>-1</sup>) for 2 hr at 10 K.

18 Note that the reported band strengths of solid H<sub>2</sub>S and D<sub>2</sub>S were obtained by

1 the transmission absorption spectroscopy (Fathe et al. 2006), while we used these values  
2 in the reflection absorption spectroscopy, which may cause some errors on the estimate  
3 of column densities. In the cases of amorphous H<sub>2</sub>O and solid CO, for example, we  
4 found that the difference in the estimated column densities between transmission and  
5 reflection methods was within a factor of two (Oba et al. 2009). Despite such potential  
6 errors on the column densities of solid H<sub>2</sub>S and D<sub>2</sub>S, we consider that the obtained  
7 parameters reported in the next section are acceptable since we focus on the variations  
8 in the relative abundances of solid H<sub>2</sub>S and D<sub>2</sub>S.

9

### 10 3. Results and Discussion

#### 11 3.1. H<sub>2</sub>S + H on p-ASW at 10–30 K

12 Figure 1 shows an FTIR spectrum of solid H<sub>2</sub>S deposited on p-ASW at 20 K,  
13 and the difference spectra after exposure to H atoms for 5 and 30 minutes. The peak at  
14 ~2570 cm<sup>-1</sup> was assigned to the S–H stretching band of solid H<sub>2</sub>S (Fathe et al. 2006).  
15 After exposure to H atoms, the magnitude of the S–H stretching band reduced, but no  
16 growth of infrared absorption bands resulting from other sulfur-bearing species was  
17 observed. In addition, no desorption of sulfur-bearing species except H<sub>2</sub>S was  
18 confirmed in the TPD experiment. These results clarify that solid H<sub>2</sub>S was lost by

1 chemical desorption from the surface. The same phenomenon was demonstrated at 10 K  
2 by Oba et al. (2018), and at 30 K in the present study (spectrum not shown).

3 Figure 2 shows the relative abundances of solid H<sub>2</sub>S on p-ASW prepared at 10,  
4 20 and 30 K as functions of atom exposure time. At each temperature, the abundance of  
5 solid H<sub>2</sub>S gradually decreased and eventually settled at ~60% of the initial abundance in  
6 the 10 and 20 K experiments, and at ~30% in the 30 K experiment. The presence of the  
7 unreacted fraction is probably due to the presence of H<sub>2</sub>S adsorbed in the potentially  
8 deep sites on ice, where the reaction of H<sub>2</sub>S with H atoms may be suppressed  
9 significantly (Oba et al. 2018). H<sub>2</sub>S loss from the ice was also confirmed in the TPD  
10 experiment (Fig. 3). The peaks at 95, 145, and 160 K are attributed to desorption of  
11 most of the weakly bound H<sub>2</sub>S from the top of the ASW surface, the H<sub>2</sub>S emitted by the  
12 molecular volcano process, and the co-desorption of H<sub>2</sub>S and H<sub>2</sub>O, respectively  
13 (Collings et al. 2004; Oba et al. 2018).

14 The effective cross section of the chemical desorption of H<sub>2</sub>S, assuming that  
15 the H<sub>2</sub>S desorbs by a single H-atom injection process, is given by Oba et al. (2018):

16 
$$\Delta[\text{H}_2\text{S}]_t/[\text{H}_2\text{S}]_0 = \alpha(1-\exp(-\sigma\phi t)), \quad (4)$$

17 where  $\Delta[\text{H}_2\text{S}]_t$  and  $[\text{H}_2\text{S}]_0$  represent the abundance variations of the solid H<sub>2</sub>S at time  $t$   
18 and the initial H<sub>2</sub>S abundance, respectively, and  $\alpha$ ,  $\sigma$ , and  $\phi$  are the saturation values of

1 the desorption fraction, the effective cross section of chemical desorption, and the atom  
2 flux, respectively. By fitting the plots in Figure 2 to Equation (4) and dividing the  
3 obtained fitting parameter by the H-atom flux, the effective cross sections  $\sigma$  of the  
4 chemical desorption from p-ASW at 10, 20 and 30 K were determined as  $(2.1 \pm 0.2) \times$   
5  $10^{-17}$ ,  $(1.3 \pm 0.1) \times 10^{-17}$ , and  $(9.6 \pm 1.2) \times 10^{-18} \text{ cm}^2$ , respectively. Note that the  
6 obtained effective cross section can be considered as the lower limit of the actual  
7 desorption cross section since the incident H-atom flux does not always cause chemical  
8 desorption. This suggests that chemical desorption is only slightly more efficient at  
9 lower temperatures than at higher temperatures. However, it should be noted that  
10 Equation (4) may oversimplify the elementary processes of H atoms on ice. Because the  
11 surface number density of H atoms markedly drops at around 20 K because of the low  
12 sticking coefficient, fewer H atoms should contribute to the surface reactions as the  
13 temperature increases under the same flux of atoms. The observed small difference in  
14 the effective cross section implies that the efficiency of chemical desorption per reactive  
15 event increases at higher temperatures.

16 By contrast, the saturation value of the desorption fraction clearly depends on  
17 the reaction temperature. At 30 K, the desorption fraction was approximately half that at  
18 10 and 20 K (Fig. 2). We first consider the effect of the solid H<sub>2</sub>S structure on the

1 reactivity, as reported previously (Hama et al. 2014). Even at low coverage, some  
2 fraction of the H<sub>2</sub>S may aggregate at the ice surface. The solid structure may also  
3 depend on the deposition temperature. Hama et al. (2014) found that H atoms react less  
4 readily with crystalline benzene than with amorphous benzene, which they attributed to  
5 geometric constraints between the two solid phases. However, the crystallization  
6 temperature in the H<sub>2</sub>S case exceeds 65 K (Fathe et al. 2006), much higher than the  
7 temperatures of the present experiment. Furthermore, we confirmed that approximately  
8 60% of the solid H<sub>2</sub>S was also released from the ice surface by chemical desorption  
9 when the sample prepared at 30 K was exposed to H atoms at 10 K. We thus conclude  
10 that the differences in solid structure arising from the sample preparation temperature do  
11 not affect the desorption fraction. We propose that the amount of non-desorbed H<sub>2</sub>S  
12 fraction is related to the residence time of the H atoms, which varies with temperature.  
13 Although the structures of the p-ASW and H<sub>2</sub>S surfaces should be considerably similar  
14 at temperatures below 30 K, the number of adsorption sites at which an H atom can  
15 remain sufficiently long for reactions (2) and (3) should decrease with increasing  
16 temperature. In particular, reaction (3), which should occur via tunneling because of the  
17 moderate energy barrier (Lamberts & Kästner 2017), requires a long residence time of  
18 H atoms at the reaction sites. At 30 K, most of the H atoms are transiently desorbed

1 from the surface, and only the H<sub>2</sub>S at relatively deeper adsorption sites can contribute to  
2 reactions (3) and (2), which may in part results in chemical desorption. Moreover, the  
3 H<sub>2</sub>S peak at 95 K in the TPD spectra of the 30 K experiment (Figure 3(b)), which is  
4 attributed to weakly bound H<sub>2</sub>S at the ASW surface, shows no signature of chemical  
5 desorption after exposure to atoms. Meanwhile, the depleted peaks at 140 and 160 K  
6 indicate chemical desorption of H<sub>2</sub>S and/or HS. By contrast, the 95 K peak in the 20 K  
7 experiment was reduced after the atom exposure, confirming that even the weakly  
8 bound H<sub>2</sub>S was desorbed by reactions with H atoms at 20 K.

9

### 10 3.2. H<sub>2</sub>S + H on p-ASW, np-ASW, and c-H<sub>2</sub>O at 10 K

11 Figure 4 shows the relative abundances of solid H<sub>2</sub>S after exposure to H atoms  
12 on the three kinds of ices at 10 K. Solid H<sub>2</sub>S was lost from all surfaces by chemical  
13 desorption. The saturation values of the desorbed fractions were considerably similar on  
14 the p-ASW and np-ASW surfaces (~60% of the initial abundance), whereas on c-H<sub>2</sub>O,  
15 the desorbed fraction saturated at approximately 80% of the initial abundance. The  
16 different abundances on ASW and c-H<sub>2</sub>O can be explained by the flatter surface of  
17 c-H<sub>2</sub>O than ASW, admitting a larger number of H-atom accessible sites.

18 Fitting the plots in Figure 4 by Equation (4), the effective desorption cross

1 sections on the p-ASW, np-ASW, and c-H<sub>2</sub>O ices at 10 K were obtained as  $(2.1 \pm 0.2) \times$   
2  $10^{-17}$ ,  $(1.6 \pm 0.2) \times 10^{-17}$ , and  $(9.4 \pm 0.7) \times 10^{-18}$  cm<sup>2</sup>, respectively. The effective  
3 desorption cross section of H<sub>2</sub>S did not strongly depend on ice structure, suggesting that  
4 H<sub>2</sub>S was effectively desorbed from all ice structures under the present experimental  
5 conditions.

6

### 7 3.3. H<sub>2</sub>S + D on p-ASW, np-ASW, and c-H<sub>2</sub>O at 10 K

8 When solid H<sub>2</sub>S was reacted with D atoms on p-ASW, np-ASW and c-H<sub>2</sub>O, the  
9 H<sub>2</sub>S abundance decreased and deuterated sulfides (HDS and D<sub>2</sub>S) were formed. These  
10 species were evidenced by the appearance of their S–D stretching band at 1860 cm<sup>-1</sup>  
11 (Figure 5). In our previous study, we confirmed that deuterated sulfides were formed on  
12 p-ASW at 10 K by the following H–D substitution reactions (Oba et al. 2018):



17 Clearly, the deuterated sulfides formed via reactions (5)–(8) on the np-ASW and c-H<sub>2</sub>O  
18 surfaces as well. At 10 K, reactions (5) and (7) must proceed by quantum tunneling

1 (Lamberts & Kästner 2017), whereas reactions (6) and (8) have no activation barrier,  
2 and therefore easily proceed at this temperature. The absorption features observed at  
3  $\sim 2500\text{ cm}^{-1}$  (Fig. 5) may be due to the O-D stretching band of  $\text{D}_2\text{O}$ , which was  
4 introduced from the D-atom source. Since the column density of the accumulated  $\text{D}_2\text{O}$   
5 was negligible ( $\sim 0.02\text{ ML}$  after 20 minutes), it would not affect the reactivity of solid  
6  $\text{H}_2\text{S}$  with D atoms on the  $\text{H}_2\text{O}$  ice. Figure 6 shows the relative peak areas of the S-H  
7 stretching band ( $\text{Area}[\text{S-H}]_t$ ) after exposure to D atoms on the three kinds of  $\text{H}_2\text{O}$  ice,  
8 normalized by the initial peak area of the S-H stretching band of  $\text{H}_2\text{S}$  ( $\text{Area}[\text{S-H}]_0$ ). As  
9 singly deuterated sulfide (HDS), which contributes to the S-H stretching band in the  
10 same region, is produced through the above reaction pathways, the variations in  
11  $\text{Area}[\text{S-H}]_t$  should be constrained by not only the decrease of  $\text{H}_2\text{S}$  but also the increase  
12 and decrease of HDS. Hence, to clarify the whole kinetics of the H-D substitution of  
13  $\text{H}_2\text{S}$ , we must quantify the abundance variations in both  $\text{H}_2\text{S}$  and HDS. However, HDS  
14 is difficult to quantify in the IR spectra because its H-S stretching band overlaps that of  
15  $\text{H}_2\text{S}$  at  $\sim 2570\text{ cm}^{-1}$ . Although the peak positions of the bending band should vary among  
16 the isotopologues, such peaks were not observed in the present study, because of the low  
17 abundances of the isotopologues ( $< 0.7\text{ ML}$ ) on the ice.

18 To simplify the discussion on the kinetics of the H-D substitution reactions, we

1 assume that the temporal variations in the  $\text{Area}[\text{S-H}]_t/\text{Area}[\text{S-H}]_0$  values during the  
2 D-atom exposure are dominated by the rate of reaction (5). That is, we assume that HDS  
3 immediately converts to  $\text{D}_2\text{S}$  and does not contribute to the observed H–S band.  
4 Although the estimation is rough, the obtained parameters should be useful for  
5 discussing the kinetics of the entire reaction system. Under such conditions, the  
6 abundance variation of  $\text{H}_2\text{S}$  in Figure 6 can be described by the following rate equation:

$$7 \quad \frac{d[\text{H}_2\text{S}]}{dt} = -k_{\text{HD}}[\text{D}][\text{H}_2\text{S}], \quad (9)$$

8 where  $[\text{D}]$  represents the abundance of D atoms on the ices, and  $k_{\text{HD}}$  is the rate constant  
9 of reaction (5). Integrating Equation (9), we get

$$10 \quad \frac{\Delta[\text{H}_2\text{S}]_t}{[\text{H}_2\text{S}]_0} = \alpha(1 - \exp(-k't)), \quad (10)$$

11 where  $\Delta[\text{H}_2\text{S}]_t$  and  $[\text{H}_2\text{S}]_0$  represent the  $\text{H}_2\text{S}$  abundance variation at time  $t$  and the initial  
12  $\text{H}_2\text{S}$  abundance, respectively, and  $k'$  ( $= k_{\text{HD}}[\text{D}]$ ) is the effective rate constant of reaction  
13 (5), which is equivalent to that of H–D substitution of  $\text{H}_2\text{S}$ . Fitting the plots in Figure 6  
14 to Equation (10), the effective rate constants on the p-ASW, np-ASW, and c- $\text{H}_2\text{O}$   
15 surfaces were calculated as  $(5.7 \pm 0.4) \times 10^{-1}$ ,  $(3.0 \pm 0.3) \times 10^{-1}$ , and  $(3.4 \pm 0.4) \times 10^{-1}$   
16  $\text{min}^{-1}$ , respectively. Since the numbers of adsorption sites on np-ASW and c- $\text{H}_2\text{O}$  are  
17 extremely similar, and lower than on p-ASW (Stevenson et al. 1999; Kimmel et al.  
18 2001), the surface number density of D atoms (denoted  $[\text{D}]$ ) may be larger on p-ASW

1 than on other kinds of ices. If  $k_{\text{HD}}$  is independent of ice structure,  $k'$  will be larger on  
2 p-ASW than on other ice surfaces. By this argument, Hidaka et al. (2007) explained the  
3 different effective rate constants of CO + H on p-ASW and c-H<sub>2</sub>O. The present study  
4 suggests that the same argument is applicable to other reaction systems. The obtained  
5 values are of the same order of magnitude as the H–D substitution reaction rates of  
6 other molecules (CH<sub>3</sub>OH, H<sub>2</sub>CO, CH<sub>3</sub>NH<sub>2</sub>, CH<sub>3</sub>CH<sub>2</sub>OH, and CH<sub>3</sub>OCH<sub>3</sub>) investigated  
7 under similar experimental conditions (e.g., surface temperature and atom flux)  
8 (Nagaoka et al. 2007; Hidaka et al. 2009; Oba et al. 2014b, 2016a,b).

9 Figure 7 shows the peak areas of the S–D stretching band of the deuterated  
10 sulfides at 1860 cm<sup>-1</sup> after exposure to D atoms on different ice surfaces. On all surfaces,  
11 the peak intensity of the S–D stretching band drastically increased after short-term  
12 exposure to D atoms, was maximized at ~10 min, and decreased with further exposure  
13 to the atoms. The earlier part of the exposure was dominated by the formation of  
14 deuterated sulfides from H<sub>2</sub>S by the H–D substitution reaction; in the latter part, the  
15 deuterated sulfides were removed from the ice surfaces by chemical desorption,  
16 described by reactions (7) and/or (8). An additional reaction (11) might also contribute  
17 to the loss of D<sub>2</sub>S by chemical desorption (Oba et al. 2018):

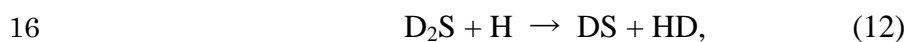


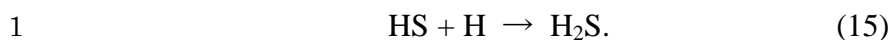
1 The formed DS radicals further react with D atoms to regain D<sub>2</sub>S (reaction 8), which  
2 may partly desorb during its formation. As clarified in the plots, the desorption of  
3 deuterated sulfides was more suppressed on p-ASW than on np-ASW and c-H<sub>2</sub>O,  
4 possibly reflecting the variable numbers and natures of the adsorption sites on different  
5 ice surfaces.

6

### 7 3.4. D<sub>2</sub>S + H on p-ASW-d

8 Figure 8 shows the FTIR spectrum of solid D<sub>2</sub>S (~0.7 ML) prepared on the  
9 p-ASW-d surface (~30 ML) at 10 K, along with the difference spectra after exposure to  
10 H atoms for 3, 5 and 20 min. The peak intensity of the S–D stretching band at ~1860  
11 cm<sup>-1</sup> decreased with increasing atom-exposure time, suggesting that the interactions  
12 with H atoms reduced the D<sub>2</sub>S abundance on the surface. Similar to the H–D  
13 substitution reactions of solid H<sub>2</sub>S, we expect that D<sub>2</sub>S exposed to H atoms undergoes  
14 successive D abstraction and H addition reactions, forming hydrogen-substituted  
15 sulfides (HDS and H<sub>2</sub>S) as follows:





2 Note that reaction (15) is identical to reaction (2). As reactions (13) and (15) are  
3 radical–radical reactions with no activation barrier, they easily proceed on the ice  
4 surface, even at 10 K. However, reactions (12) and (14), with activation barriers of  
5  $\sim 1800$  and  $\sim 1500$  K, respectively (Lamberts & Kästner 2017), can proceed only by  
6 quantum tunneling at 10 K. The formed hydrogen-substituted sulfides are not clarified  
7 at  $\sim 2570 \text{ cm}^{-1}$  in the difference spectra, as their S–H band is obscured by variations in  
8 the O–D stretching band of p-ASW-d in the same region (Fig. 8b). We preliminary  
9 confirmed that the S–H stretching band of pure solid  $\text{D}_2\text{S}$  grows under exposure to H  
10 atoms on a gold-coated metal substrate at 10 K (Fig. 8c). Based on these results, we are  
11 confident that the D–H substitution of  $\text{D}_2\text{S}$  proceeds after interactions with H atoms,  
12 even on p-ASW-d.

13 Figure 9 plots the relative peak area of the S–D stretching band versus the  
14 exposure time to H-atoms (the results of  $\text{H}_2\text{S}$  after exposure to D atoms on p-ASW are  
15 also shown for comparison). Assuming that the intermediate species HDS contributes  
16 insignificantly to the decrease of the S–D stretching band, the plots in Figure 9  
17 approximately show the variations in the relative abundance of  $\text{D}_2\text{S}$  dissociated by  
18 reaction (12) only. Under those conditions, the kinetic parameters of the D–H

1 substitution reactions can be obtained by fitting the plots of Figure 9 to the following  
2 equation:

$$3 \quad \Delta[\text{D}_2\text{S}]_t/[\text{D}_2\text{S}]_0 = \alpha(1-\exp(-k_{\text{DH}}[\text{H}]t)), \quad (16)$$

4 where  $\Delta[\text{D}_2\text{S}]_t$  and  $[\text{D}_2\text{S}]_0$  represent the variation in the  $\text{D}_2\text{S}$  abundance at time  $t$  and the  
5 initial  $\text{D}_2\text{S}$  abundance, respectively, and  $k_{\text{DH}}$  and  $[\text{H}]$  represent the rate constant of  
6 reaction (12) and the surface number density of H atoms on the ice, respectively. As  $[\text{H}]$   
7 cannot be measured under the present experimental conditions,  $k_{\text{DH}}$  cannot be isolated  
8 from the fitting parameter. Instead, the fitting parameter  $k_{\text{DH}}[\text{H}]$  ( $= k''$ ) is defined as the  
9 effective rate constant of reaction (12), equivalent to that of D–H substitution of  $\text{D}_2\text{S}$ .  
10 Accordingly, by comparing  $k''$  and  $k'$ , we can discuss the possible isotope effects on the  
11 H–D and D–H substitution reactions.

12 The effective rate constant  $k''$  was calculated as  $(1.4 \pm 0.1) \times 10^{-1}$  minutes<sup>-1</sup>,  
13 approximately one-quarter that of  $k'$  ( $5.7 \times 10^{-1}$  minutes). According to Kuwahata et al.  
14 (2015), the number density ratio of D and H atoms ( $[\text{D}]/[\text{H}]$ ) on the p-ASW surface in  
15 the present flux regime ( $\sim 1\text{--}2 \times 10^{14}$  atoms cm<sup>-2</sup> s<sup>-1</sup>) is approximately 3. Therefore, the  
16 isotope effect on the H–D and D–H substitution reactions ( $k_{\text{HD}}/k_{\text{DH}}$ ) can be calculated by  
17 rearranging the relationship  $k'/k'' = k_{\text{HD}}[\text{D}]/k_{\text{DH}}[\text{H}]$  as follows:

$$18 \quad k_{\text{HD}}/k_{\text{DH}} = 1/3 \times k'/k'' = 1.35.$$

1 Lamberts and Kästner (2017) theoretically estimated the isotope effect on the same  
2 reaction system at 55–240 K. Assuming that these reactions proceed by quantum  
3 tunneling, the reaction rate is temperature-independent, especially in the  
4 low-temperature regime. Hence, the relative reaction rate at 55 K would not  
5 significantly differ from that at lower temperatures (such as 10 K). Lamberts and  
6 Kästner (2017) calculated the values of  $k_{\text{HD}}$  and  $k_{\text{DH}}$  at 55 K ( $1.07 \times 10^6 \text{ s}^{-1}$  and  $7.50 \times$   
7  $10^5 \text{ s}^{-1}$ , respectively, in Table S4 in their article), resulting in the  $k_{\text{HD}}/k_{\text{DH}}$  ratio as  $(1.07 \times$   
8  $10^6)/(7.50 \times 10^5) = 1.43$ , which excellently agrees with our experimental value.

9

## 10 4. Astrochemical Implications

### 11 4.1 Chemical desorption of H<sub>2</sub>S

12 Recently, we demonstrated that chemical desorption removes H<sub>2</sub>S from  
13 interstellar icy grains more effectively than photodesorption, releasing H<sub>2</sub>S and/or HS  
14 into the gas phase even at 10 K (Oba et al. 2018). However, it remains to be clarified  
15 whether chemical desorption effectively proceeds when H<sub>2</sub>S and H atoms react on  
16 np-ASW, which is thought to be representative of H<sub>2</sub>O structures in dense clouds, as  
17 so-called dangling OH bands have not been detected in astronomical observations  
18 (Smith et al. 1989). Minissale et al. (2016) explored chemical desorption from np-ASW

1 in laboratory studies and proposed that several molecules could desorb during their  
2 formation. The present results similarly showed that H<sub>2</sub>S can be released into the gas  
3 phase via chemical desorption on np-ASW (Fig. 4). Moreover, the effective desorption  
4 cross section (an indicator of desorption efficiency) is equivalent to that of p-ASW.

5 In our previous study, we estimated the desorption efficiency per incident H  
6 atom as  $5.4 \times 10^{-3}$ , under an H-atom flux of  $1.3 \times 10^{14}$  atoms cm<sup>-2</sup> s<sup>-1</sup> (Oba et al. 2018).  
7 For comparison, we here calculate the desorption efficiency per incident H atom (in  
8 molecules atoms<sup>-1</sup>) under the same experimental conditions (i.e. on p-ASW at 10 K).  
9 Dividing the H<sub>2</sub>S decrease during the initial 10 minutes ( $2.3 \times 10^{14}$  molecules cm<sup>-2</sup>) by  
10 the H-atom fluence over the same duration ( $3.4 \times 10^{14}$  atoms cm<sup>-2</sup>), we obtain  $6.7 \times 10^{-3}$ ,  
11 similar to the previous value. Although this argument is not verifiable under the present  
12 experimental conditions, if the H<sub>2</sub>S desorbs via reaction (2) only, the desorption  
13 efficiency would be double that of the calculated one ( $\sim 1.3 \times 10^{-2}$ ), because the number  
14 of available H atoms in reaction (2) is at most half the total atom fluence. If the  
15 calculated value is equivalent to the lower limit of the desorption efficiency per reactive  
16 event, as defined in chemical modeling studies (Garrod et al. 2007; Furuya et al. 2013),  
17 then our value exceeds the value  $8 \times 10^{-3}$  commonly assumed in models (Wakelam et al.  
18 2017; K. Furuya, 2018, private communication). Furthermore, the experimentally

1 determined lower limit is probably lower than that in actual interstellar clouds, because  
2 most of the H atoms landed on the ice surface would recombine in the laboratory  
3 experiment, lowering the number of H atoms available for reactions with H<sub>2</sub>S and HS.  
4 Hence, we again conclude that H<sub>2</sub>S can be released from icy grains via chemical  
5 desorption at higher efficiencies than hitherto expected. Accordingly, H<sub>2</sub>S desorption  
6 should be an important source of gaseous H<sub>2</sub>S in cold dense clouds, regardless of the ice  
7 structures on the grains.

8

#### 9 4.2. Contribution to deuterated sulfides in the ISM

10 Deuterated sulfides have been detected in the ISM (van Dishoeck et al. 1995;  
11 Vastel et al. 2003). The observed abundances of HDS and D<sub>2</sub>S relative to H<sub>2</sub>S are 10<sup>-1</sup>  
12 toward IRAS16293–2422 (van Dishoeck et al. 1995) and of the order of 10<sup>-2</sup> toward  
13 class 0 sources and dense cores (Vastel et al. 2003). The deuteration levels of sulfide  
14 species are significantly higher than the cosmic abundance of D atoms ( $\sim 1 \times 10^{-5}$ ;  
15 Linsky 2003) and the deuteration levels of ISM water (HDO/H<sub>2</sub>O  $\sim 3 \times 10^{-2}$ , D<sub>2</sub>O/H<sub>2</sub>O  $\sim$   
16  $1 \times 10^{-3}$ , Coutens et al. 2012, 2014; Vastel et al. 2010). The different deuteration levels  
17 of H<sub>2</sub>S and H<sub>2</sub>O are probably attributable to their different deuteration pathways: H<sub>2</sub>O is  
18 deuterated during its formation process only (Oba et al. 2012; Taquet et al. 2013),

1 whereas H<sub>2</sub>S, once formed on grains, can also be deuterated through H–D substitution  
2 processes. Therefore, the deuteration level of H<sub>2</sub>S can potentially exceed the atomic  
3 D/H ratio in the environment. It is widely recognized that H–D substitution reactions on  
4 grains enrich the deuterium contents of various interstellar molecules, such as methanol  
5 and formaldehyde (Nagaoka et al. 2007; Hidaka et al. 2009; Taquet et al. 2013). In  
6 particular, the heavily deuterated signature of methanol toward class 0 protostars (e.g.,  
7 CH<sub>2</sub>DOH/CH<sub>3</sub>OH > 0.4, Parise et al. 2006) reflects the extremely low occurrence of D–  
8 H substitution in methanol, meaning that its deuteration level remains high (Nagaoka et  
9 al. 2007). In other words, once deuterated methanol such as CH<sub>2</sub>DOH and CHD<sub>2</sub>OH is  
10 formed through the H–D substitution reactions of CH<sub>3</sub>OH, it never returns to the  
11 original non-deuterated methanol, which explains the significant deuterium enrichment  
12 of interstellar methanol. By contrast, hydrogen sulfides undergo both H–D and D–H  
13 substitution on icy surfaces at 10 K (Figs. 5 and 8). In addition, the isotope effect is not  
14 significant ( $k'/k'' \sim 1.4$ ). The atomic D/H ratio in dense clouds is generally much lower  
15 than unity (Roberts et al. 2004), implying that any deuterated sulfides formed by H–D  
16 substitution from H<sub>2</sub>S are restored to H<sub>2</sub>S through reactions with abundant H atoms on  
17 grains. This mechanism may in principle suppress the deuteration level of H<sub>2</sub>S.  
18 However, once HDS is formed from H<sub>2</sub>S via H–D substitution (reactions 5 and 6), it

1 may be released into the gas phase via chemical desorption. The desorbed HDS  
2 undergoes D–H substitution through reactions (14) and (15) only when re-adsorbed onto  
3 the grain surfaces, which might explain the relatively high deuteration levels of H<sub>2</sub>S in  
4 the ISM.

5

## 6 5. Concluding Remarks

7 We experimentally demonstrated that H<sub>2</sub>S can be released from various ice  
8 structures via chemical desorption at low temperatures. The effective desorption  
9 cross-section depends little on the ice structure and temperature. On the contrary, the  
10 degree of the desorbed fraction is influenced by both parameters, probably because the  
11 number and nature of the adsorption sites vary on ices with different textures. The  
12 present experimental results strongly suggest that the desorption efficiency per reactive  
13 event, which was estimated from the first linear part of the reaction, is much larger than  
14 that typically applied in modeling studies.

15 At 10 K, both H–D and D–H substitutions of hydrogen sulfides occur by  
16 tunneling atom-abstraction followed by barrierless atom addition. The isotope effect on  
17 the H–D and D–H substitution reactions was estimated from the ratio of the effective  
18 rate constants of the substitution reactions and the number density ratio of the D and H

1 atoms. The result was 1.4, meaning that the H–D substitution is slightly faster than D–H  
2 substitution on the p-ASW surface at 10 K. Note that the isotope effect was estimated  
3 on an assumption that the intermediate species HDS insignificantly contributed to the  
4 quantification of H<sub>2</sub>S and D<sub>2</sub>S. This small isotope effect excellently agreed with the  
5 theoretical value (also 1.4). Although the deuterated sulfides on grains will likely  
6 transform into their hydrogenated forms through D–H substitution, the deuteration  
7 levels of hydrogen sulfides in the gas phase may be maintained by chemical desorption  
8 upon the formation of deuterated sulfides.

9

## 10 Acknowledgment

11 The authors appreciated the consecutive review by an anonymous reviewer, which was  
12 helpful to improve the earlier version of the manuscript. The authors thank Dr. T.  
13 Lamberts at Leiden University, Dr. K. Furuya at University of Tsukuba, and Dr. W. M.  
14 C. Sameera at Hokkaido University for discussion on the surface reactivity and  
15 chemical desorption of H<sub>2</sub>S. The authors also thank Dr. T. Hama at Hokkaido University  
16 for helpful comments on the preparation of H<sub>2</sub>O ices. This work was partly supported  
17 by JSPS KAKENHI Grant Nos. JP26707030, JP17H06087, and JP17H04862.

18

1 Figure captions

- 2 Fig. 1 FTIR spectrum of solid H<sub>2</sub>S (~0.7 ML) deposited on p-ASW (~30 ML) at 20 K  
3 (top), and the difference spectra after exposure to H atoms for 5 minutes  
4 (center) and 30 minutes (bottom).
- 5 Fig. 2 Relative abundances of solid H<sub>2</sub>S on p-ASW versus atom exposure time at 10K  
6 (black), 20 K (red), and 30 K (blue). The solid lines are the least-squares  
7 fittings of the plots by Equation (4).
- 8 Fig. 3 TPD spectra ( $m/z = 34$ ) of remaining solid H<sub>2</sub>S after exposure to H atoms (a) at  
9 20 K and (b) 30 K (solid red lines). The dashed lines are the TPD spectra  
10 obtained after exposure to H<sub>2</sub> molecules only (blank experiment) at each  
11 temperature.
- 12 Fig. 4 Relative abundances of solid H<sub>2</sub>S on three kinds of ices (p-ASW, np-ASW, and  
13 c-H<sub>2</sub>O) versus atom exposure time at 10 K.
- 14 Fig. 5 FTIR spectrum of solid H<sub>2</sub>S (~0.7 ML) deposited on np-ASW (~30 ML) at 10 K  
15 (upper panel), and the difference spectra after exposure to D atoms for 20 s, 3  
16 minutes, and 20 minutes (top to bottom in lower panel).
- 17 Fig. 6 Peak areas of the S–H stretching band of H<sub>2</sub>S after exposure to D atoms on the  
18 three kinds of ices at 10 K. The values along the Y-axis are defined and  
19 interpreted in the main text. The solid lines are the least-squares fitting of the  
20 plots by Equation (10).
- 21 Fig. 7 Peak area of the S–D stretching band observed at 1860 cm<sup>-1</sup> after exposure to D  
22 atoms on the three ice surfaces. The solid lines are guides for the eyes.
- 23 Fig. 8 (a) FTIR spectrum of solid D<sub>2</sub>S (~0.7 ML) prepared on p-ASW-d (~30 ML) at 10  
24 K, (b) difference spectra after exposure to H atoms for 3 minutes (top), 5  
25 minutes (center), and 20 minutes (bottom), (c) difference spectrum of solid D<sub>2</sub>S  
26 after exposure to H atoms for 80 minutes on Au substrate at 10 K (shown for  
27 comparison). The inset in (a) is an enlargement of the spectrum focusing on the  
28 S–D stretching band of D<sub>2</sub>S (1860 cm<sup>-1</sup>).
- 29 Fig. 9 Relative peak area of the S–D stretching band versus H-atom exposure time at 10  
30 K (blue). The relative peak area of the S–H stretching band of H<sub>2</sub>S after  
31 exposure to D atoms on p-ASW (black) is plotted for comparison. The solid  
32 lines are the least-squares fitting of the plots by Equation (10) or (16).  
33  
34  
35

1  
2 References  
3 Chuang K.-J., Fedoseev G., Qasim D., Ioppolo S., van Dishoeck E. F., & Linnartz H.  
4 2018, *ApJ*, 853, 102.  
5 Collings M. P., et al. 2004, *MNRAS*, 354, 1133.  
6 Coutens A., et al. 2012, *A&A*, 539, A132.  
7 Coutens A., et al. 2014, *ApJL*, 792, L5.  
8 Cuppen H. M., et al. 2017, *SSRv*, 212, 1.  
9 Dulieu, F., et al. 2013, *Sci. Rep.* 3, 1338.  
10 Fathe K., Holt J. S., Oxley S. P., & Pursel, C. J. 2006, *J. Phys. Chem. A*, 110, 10793.  
11 Furuya K., Aikawa Y., Nomura H., Hersant F., & Wakelam V. 2013, *ApJ*, 779, 11.  
12 Garrod, R. T., Wakelam, V. & Herbst, E. 2007, *A&A*, 467, 1103.  
13 Geballe T. R., Baas F., Greenberg J. M., & Schutte W. 1985, *A&A*, 146, L6.  
14 Hama T., Ueta H., Kouchi A., Watanabe N., & Tachikawa H. 2014, *JPCL*, 5, 3843.  
15 Hatchell J., Thompson M. A., Millar T. J., & Macdonald G. H. 1998, *A&A*, 338, 713.  
16 He J., Emtiaz S. M., & Vidali G. 2017, *ApJ*, 851, 104.  
17 Hidaka H., Kouchi A., & Watanabe N. 2007, *JCP*, 126, 204707.  
18 Hidaka H., Watanabe M., Kouchi A., & Watanabe N. 2009, *ApJ*, 702, 291.  
19 Jiménez-Escobar, A. & Muñoz Caro, G. M. 2011, *A&A*, 536, A91.  
20 Kimmel G. A., Stevenson K. P., Dohnálek Z., Scott Smith R., & Kay B. D. 2001, *JCP*,  
21 114, 5284.  
22 Kuwahata K., Hama T., Kouchi A., & Watanabe N. 2015, *PRL*, 115, 133201.  
23 Lamberts T., & Kästner J. 2017, *JPCA*, 121, 9736.  
24 Linsky, J. L. 2003, *SSRv*, 106, 49.  
25 Millar T. J., Adams N. G., Smith D., Lindinger W., & Villinger H. 1986, *MNRAS*, 221,  
26 673.  
27 Millar T. J., & Herbst E. 1990, *A&A*, 231, 466.  
28 Minh, Y. C., Irvine W. M., & Ziurys L. M. 1989, *ApJL*, 345, L63.  
29 Minissale, M., Dulieu, F., Cazaux, S. & Hocuk, S. 2016, *A&A*, 585, A24.  
30 Nagaoka, A., Watanabe, N., & Kouchi, A. 2007, *JPCA*, 111, 3016.  
31 Neufeld D. A., et al. 2015, *A&A*, 577, A49.  
32 Oba Y., et al. 2009, *ApJ*, 701, 464.  
33 Oba Y., Osaka K., Watanabe N., Chigai T., & Kouchi A. 2014a, *Faraday Discuss.*, 168,  
34 185.  
35 Oba Y., Chigai T., Osamura Y., Watanabe N., & Kouchi A., 2014b, *MAPS*, 49, 117.  
36 Oba Y., Watanabe N., & Kouchi A. 2016a, *Chem. Phys. Lett.*, 662, 14.

1 Oba Y., Osaka K., Chigai T., Kouchi A., & Watanabe N. 2016b, MNRAS, 462, 689.  
2 Oba Y., Watanabe N., Hama T., Kuwahata K., Hidaka H., & Kouchi A. 2012, ApJ,  
3 749,67.  
4 Oba Y., Tomaru T., Lamberts, T., Kouchi A., & Watanabe N. 2018, Nat. Astron., 2, 228.  
5 Parise B., et al. 2006, A&A, 453, 949.  
6 Phuong N. T., et al. 2018, A&A, 616, L5.  
7 Roberts H., Herbst E., Millar T. J., 2004, A&A, 424, 905.  
8 Smith, R. G., Sellgren K., & Tokunaga A. T. 1989, ApJ, 344, 413.  
9 Stevenson K. P., Kinnel G. A., Dohnálek Z., Scott Smith R., & Kay B. D. 1999, Sci.,  
10 283, 1505.  
11 Taquet V., et al. 2013, A&A, 550, A127.  
12 Thaddeus, P., Kutner M. L., Penzias A. A., Wilson R. W., & Jefferts K. B. 1972, ApJL,  
13 176, L73.  
14 van Dishoeck, E. F., Blake, G. A. Jansen, D. J. & Groesbeck, T. D. 1995, ApJ, 447, 760.  
15 Vastel C., Phillips, T. G., Ceccarelli, C., & Pearson J. 2003, ApJL, 596, L97.  
16 Vastel C., et al. 2010, A&A, 521, L31.  
17 Wakelam V., et al. 2004, A&A, 413, 609.  
18 Wakelam V., Loison J.-C., Mereau R., & Ruaud M. 2017, Mol. Astrophys., 6, 22.  
19  
20

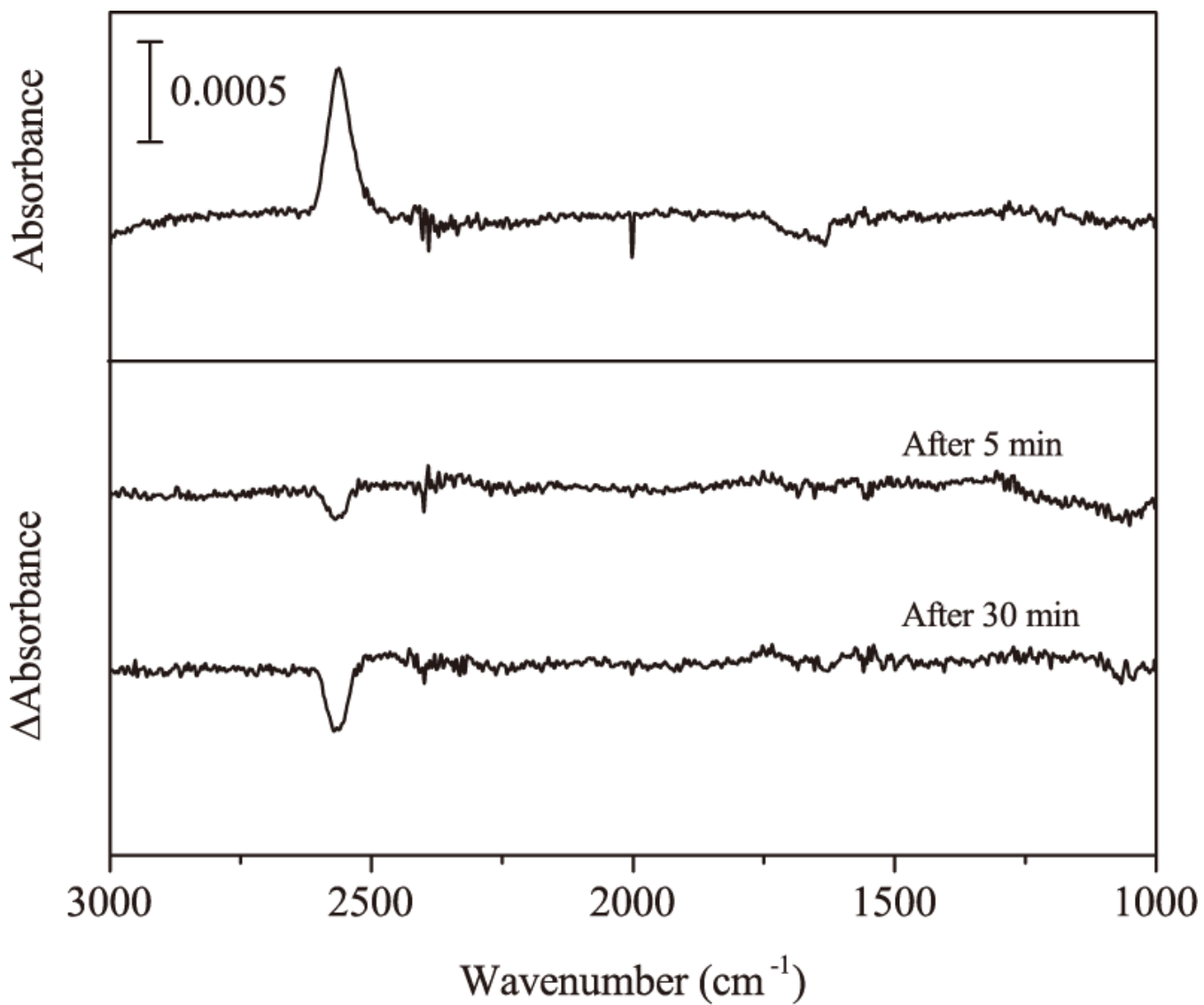


Figure 1

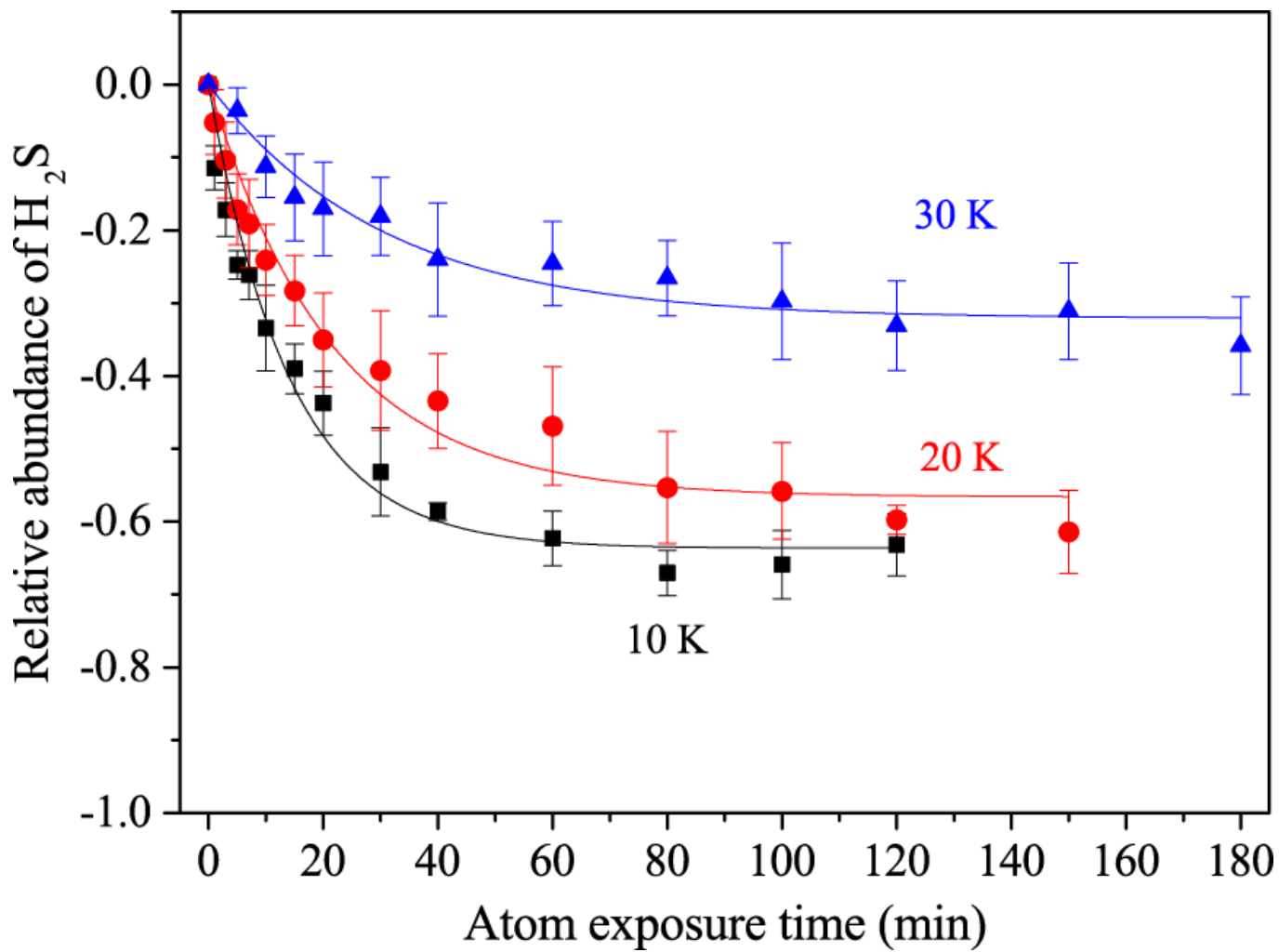


Figure 2

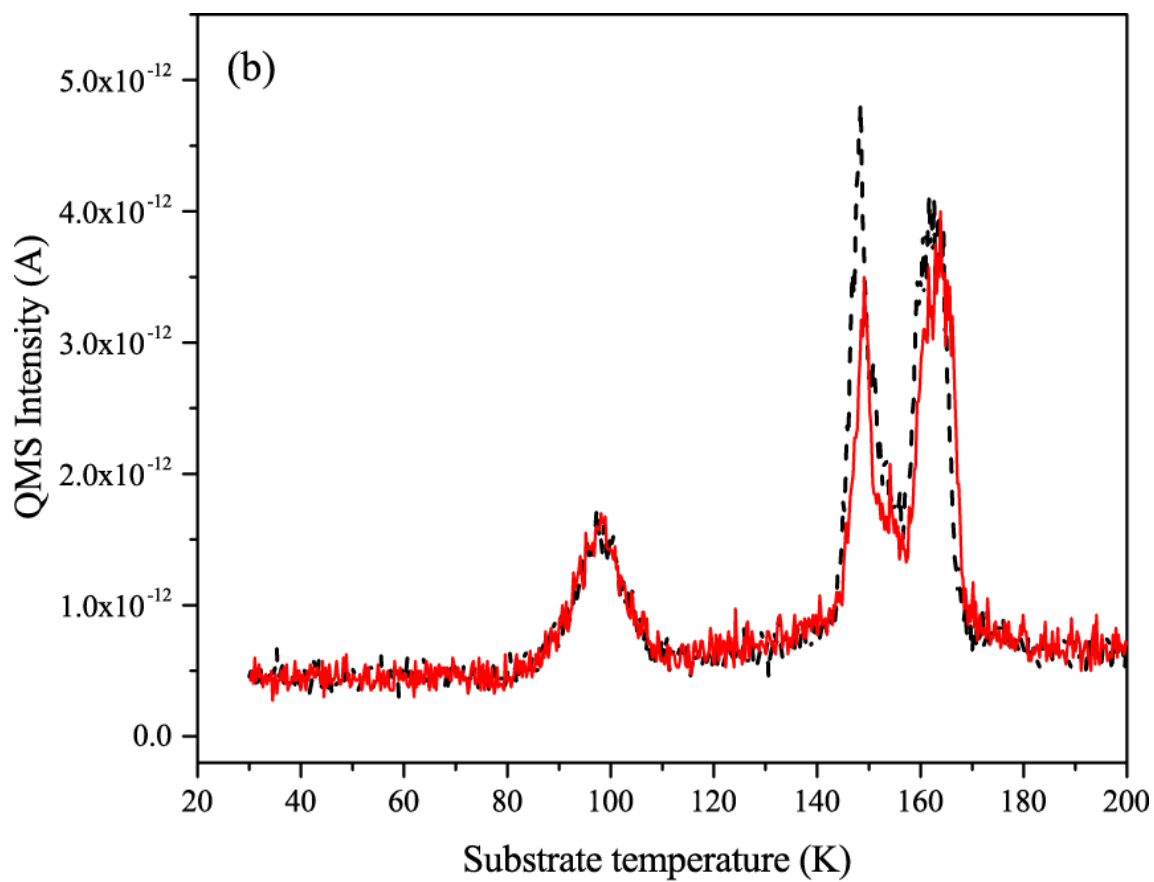
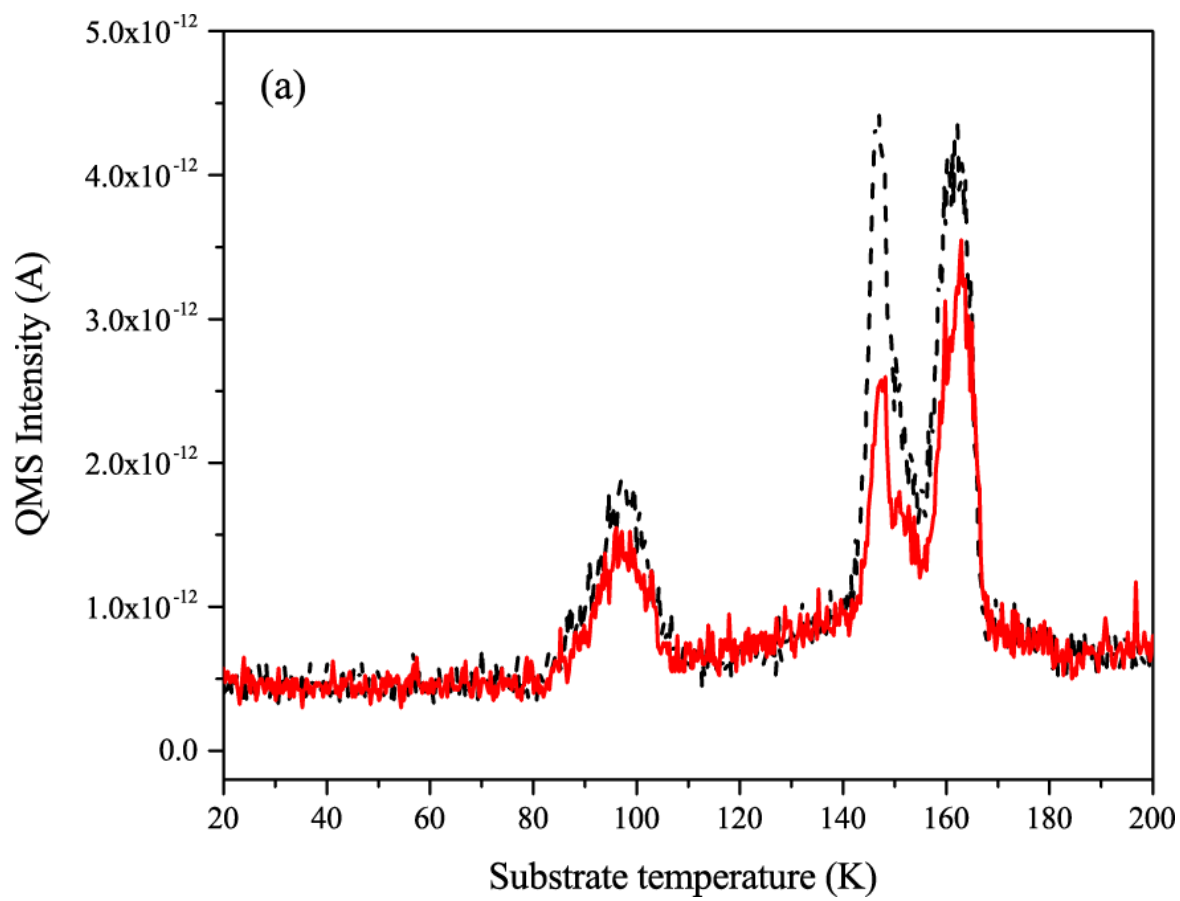


Figure 3

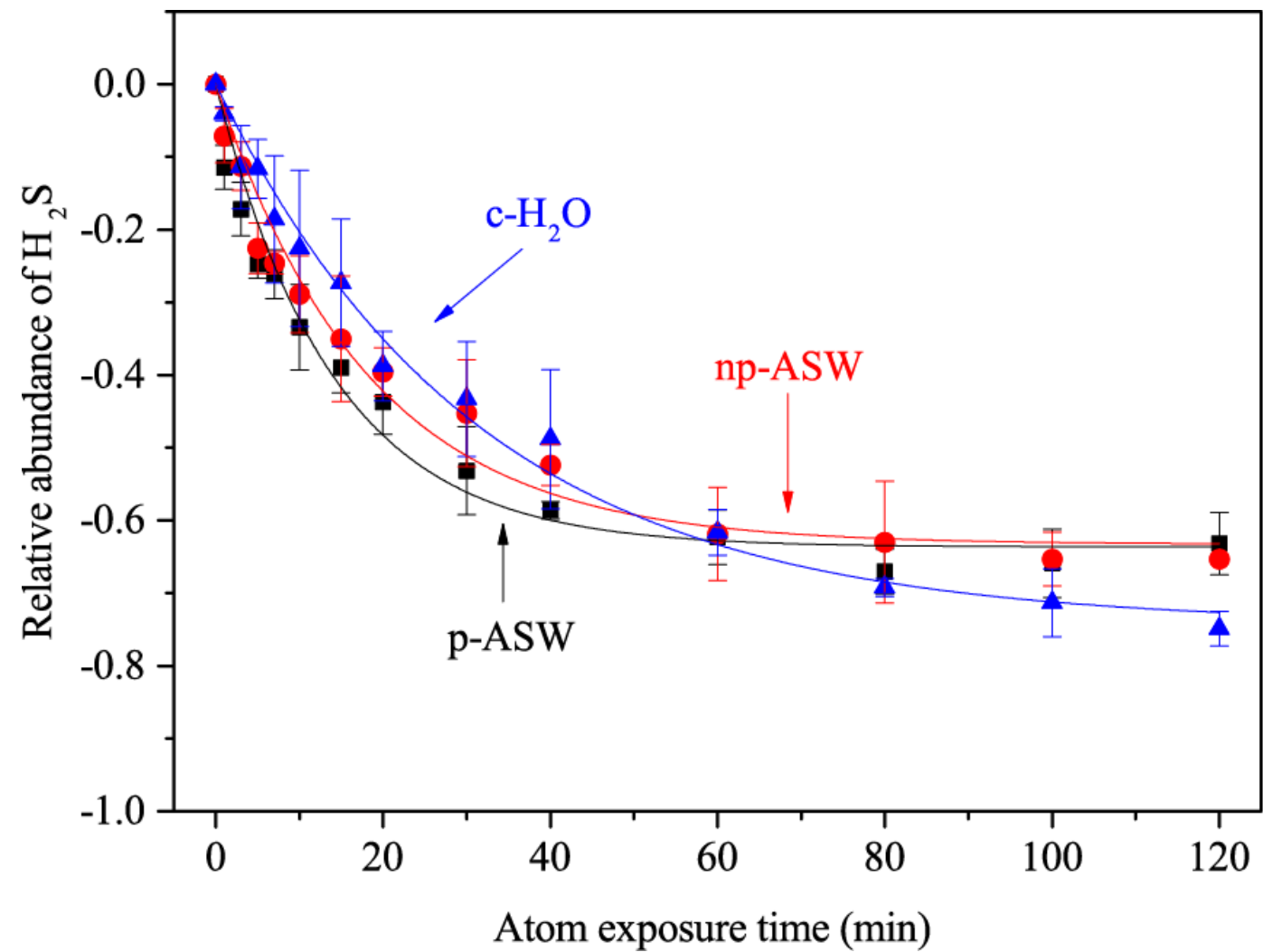


Figure 4

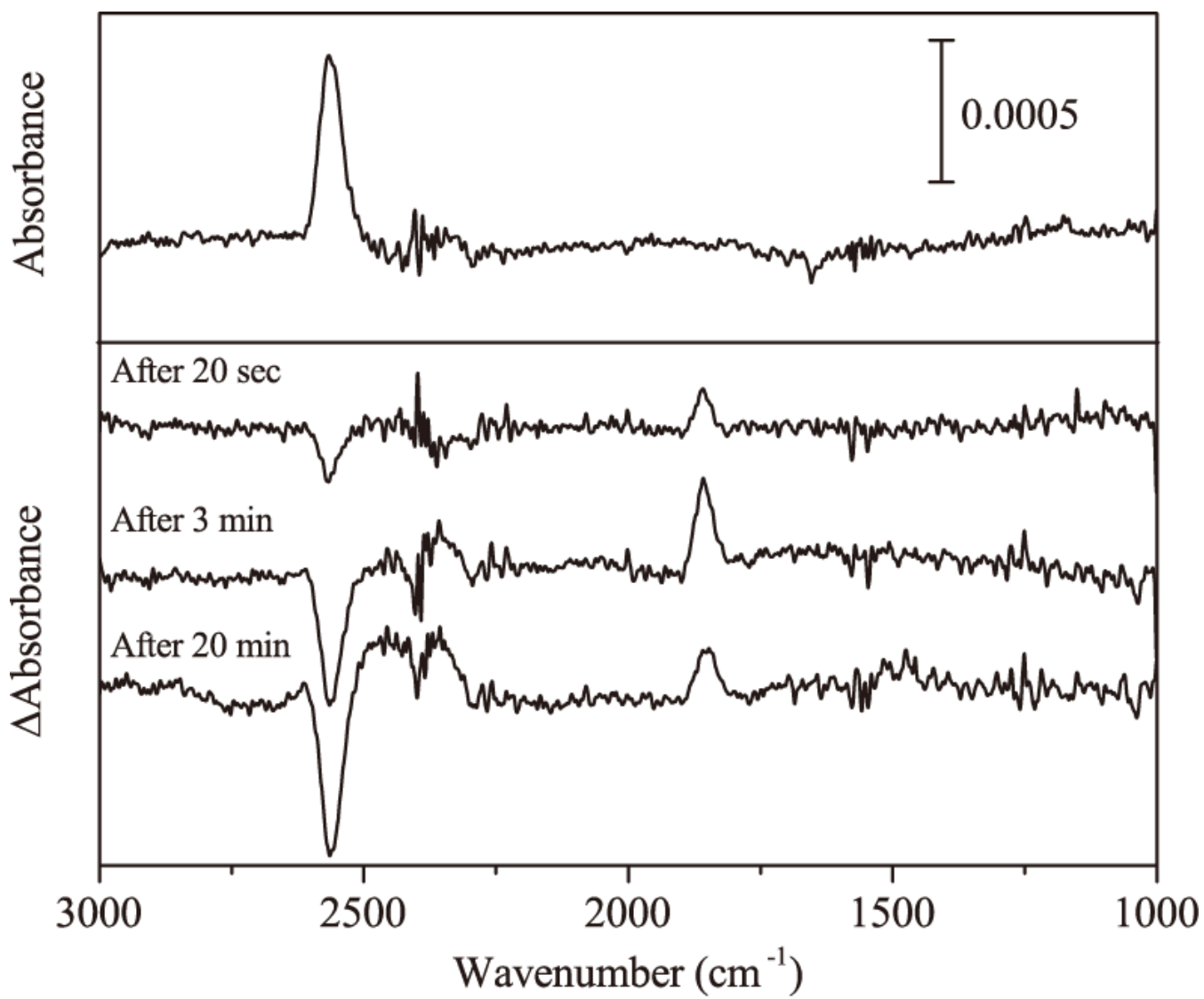


Figure 5

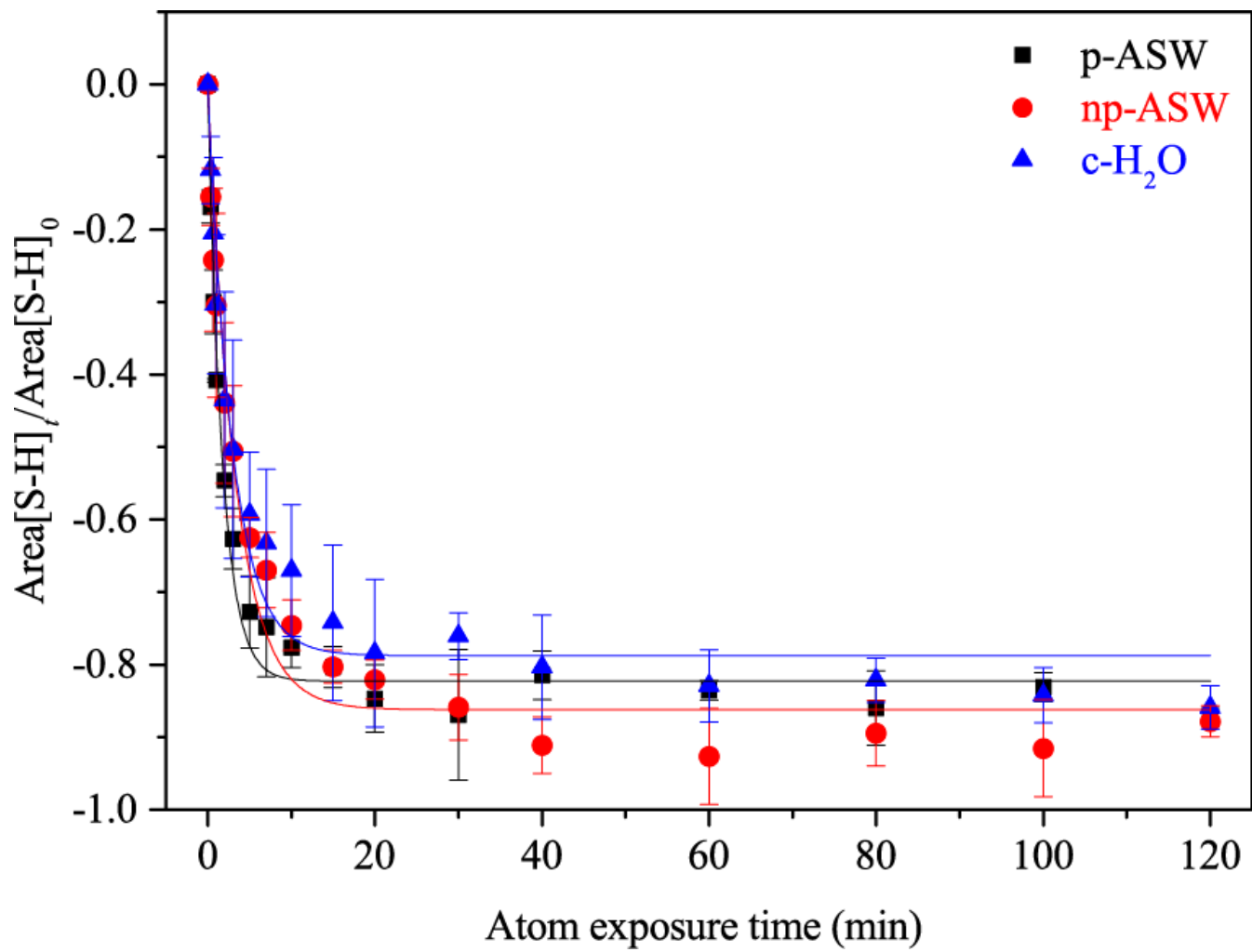


Figure 6

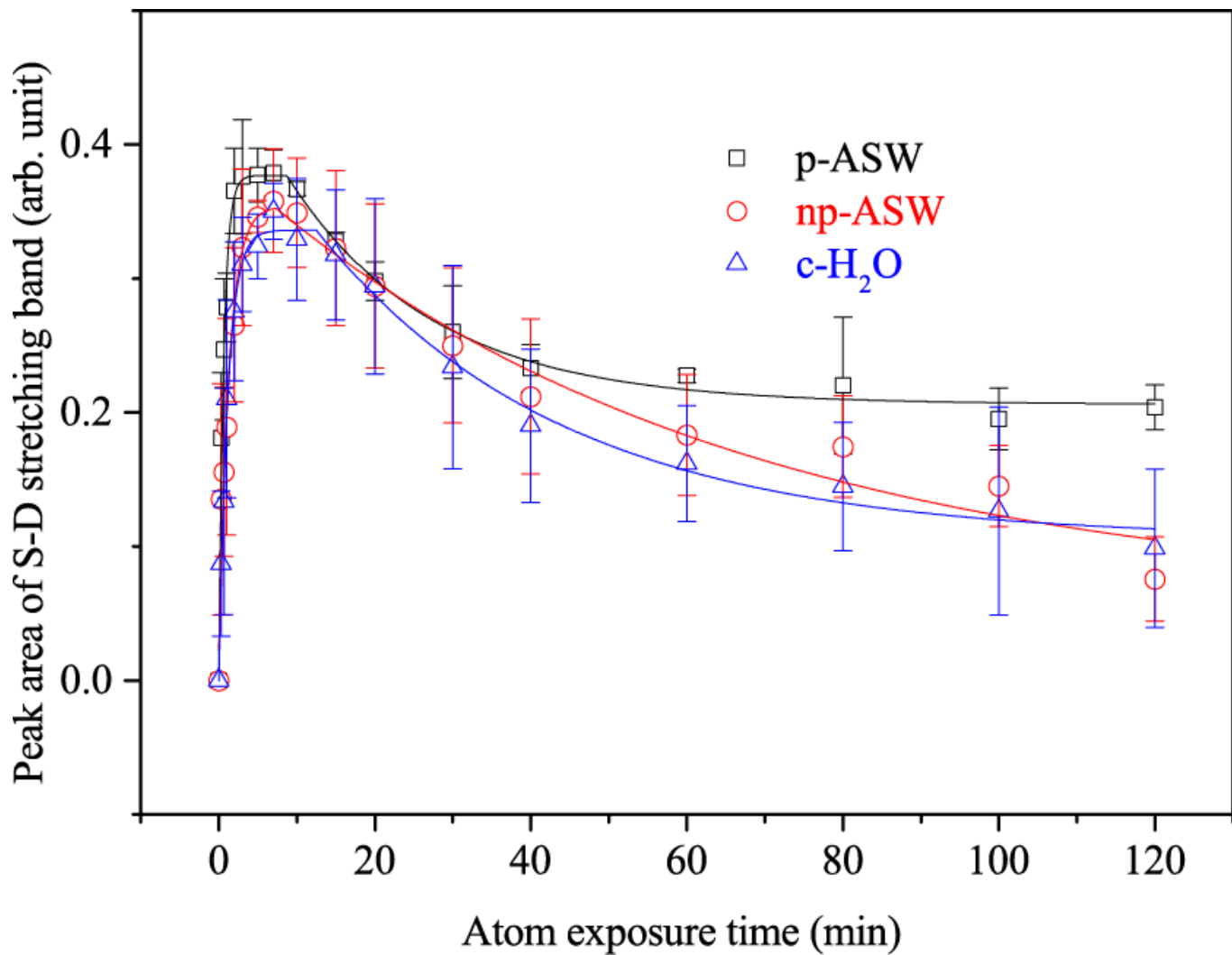


Figure 7

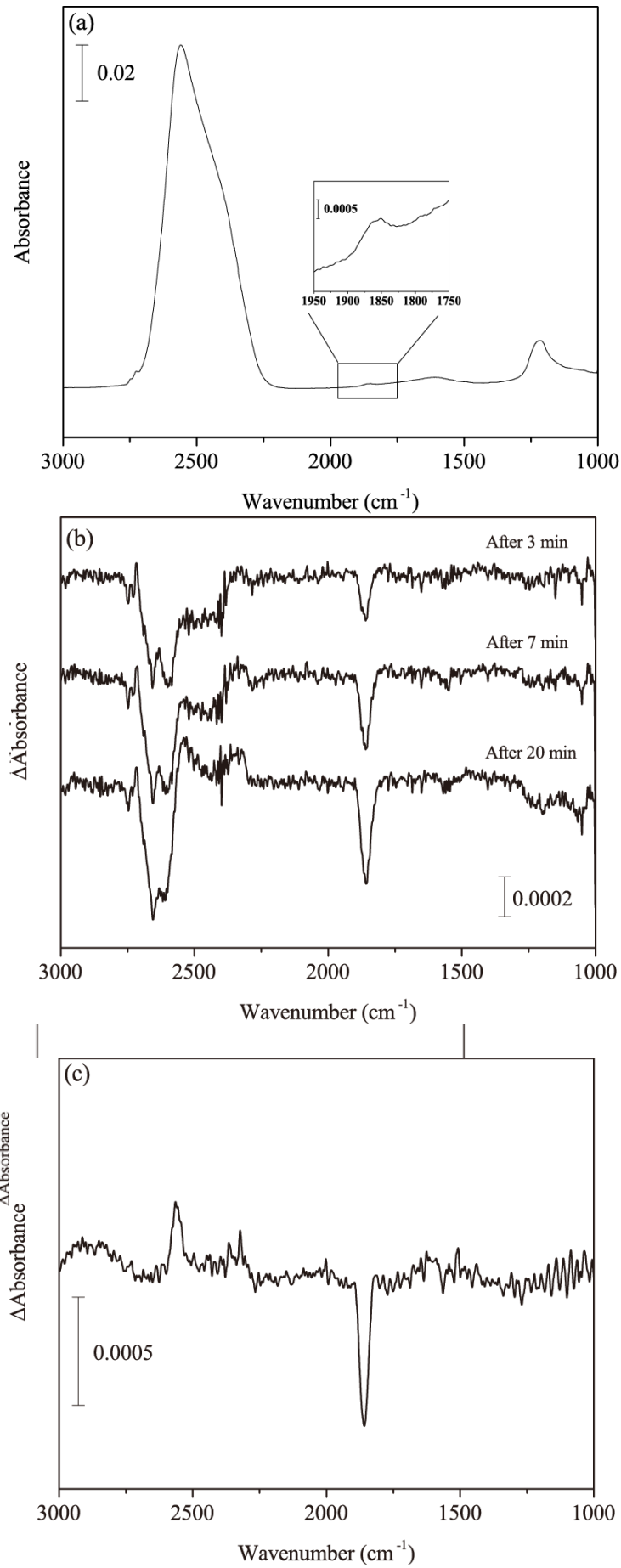


Figure 8

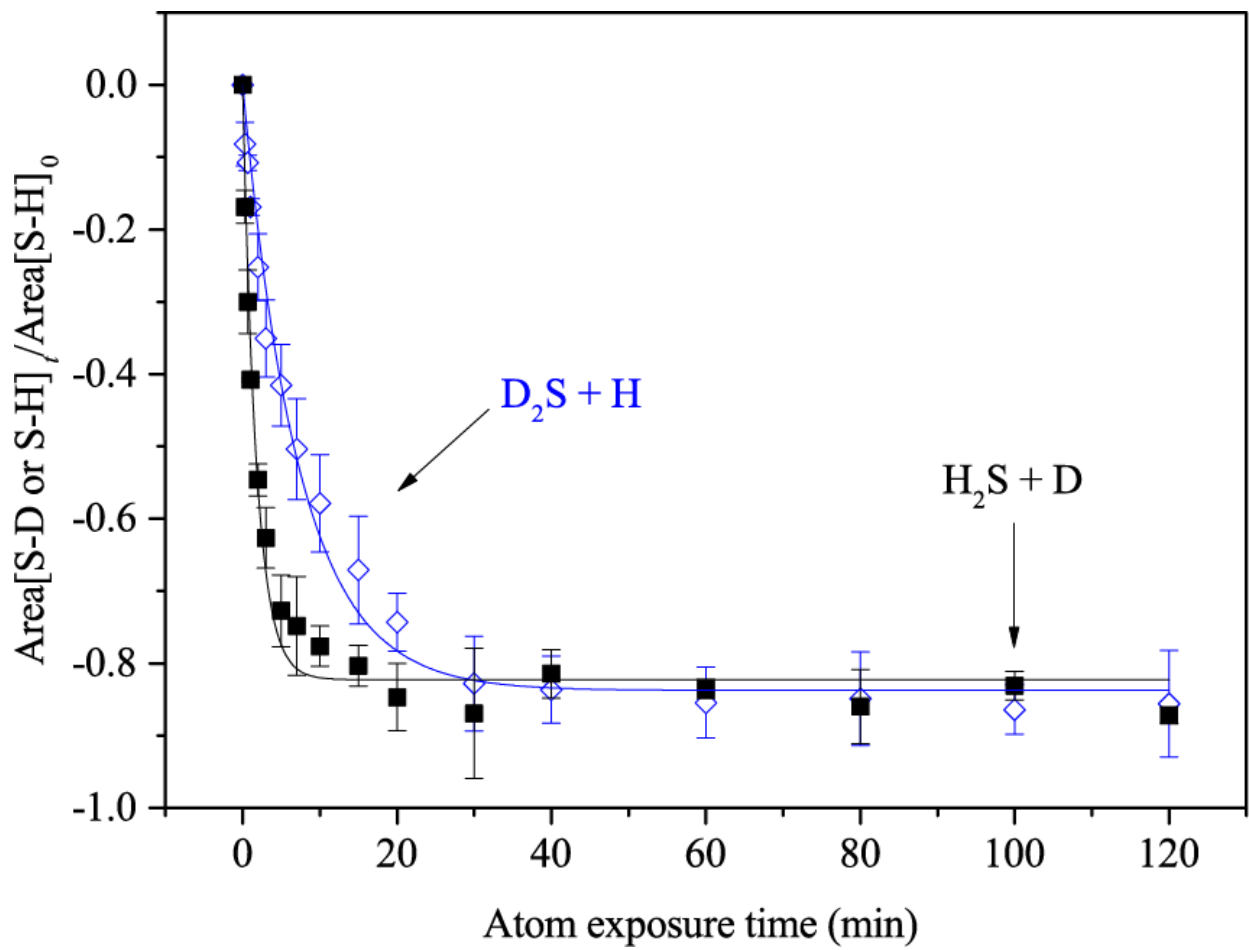


Figure 9